

Abrupt enhancement of noncentrosymmetry and appearance of a spin-triplet superconducting state in $\text{Li}_2(\text{Pd}_{1-x}\text{Pt}_x)_3\text{B}$ beyond $x = 0.8$

S. Harada,¹ J. J. Zhou,² Y. G. Yao,^{2,3,*} Y. Inada,⁴ and Guo-qing Zheng^{1,2,†}

¹*Department of Physics, Okayama University, Okayama 700-8530, Japan*

²*Institute of Physics and Beijing National Laboratory for Condensed Matter Physics, Chinese Academy of Sciences, Beijing 100190, China*

³*School of Physics, Beijing Institute of Technology, Beijing 100081, China*

⁴*Department of Science Education, Faculty of Education, Okayama University, Okayama 700-8530, Japan*

(Received 12 July 2012; revised manuscript received 20 November 2012; published 3 December 2012)

We report synthesis, ¹⁹⁵Pt, ¹¹B, and ⁷Li NMR measurements, and first-principles band calculations for noncentrosymmetric superconductors $\text{Li}_2(\text{Pd}_{1-x}\text{Pt}_x)_3\text{B}$ ($x = 0, 0.2, 0.5, 0.8, 0.84, 0.9$, and 1). For $0 \leq x \leq 0.8$, the spin-lattice relaxation rate $1/T_1$ shows a clear coherence peak just below T_c , decreasing exponentially at low temperature, and the Knight shift ¹⁹⁵K decreases below T_c . For $x = 0.9$ and 1.0 , in contrast, $1/T_1$ shows no coherence peak but a T^3 variation and ¹⁹⁵K remains unchanged across T_c . These results indicate that the superconducting state changes drastically from a spin-singlet dominant to a spin-triplet dominant state at $x = 0.8$. We find that the distortion of $\text{B}(\text{Pt},\text{Pd})_6$ increases abruptly above $x = 0.8$, which leads to an abrupt enhancement of the asymmetric spin-orbit coupling as confirmed by band calculation. Such structure distortion that enhances the extent of inversion-symmetry breaking is primarily responsible for the pairing symmetry evolution. The insight obtained here provides a guideline for searching for noncentrosymmetric superconductors with a large spin-triplet component.

DOI: [10.1103/PhysRevB.86.220502](https://doi.org/10.1103/PhysRevB.86.220502)

PACS number(s): 74.25.N- , 71.70.Ej, 74.25.Jb, 76.60.Cq

The superconducting state in materials without spatial inversion symmetry has been a very popular topic in condensed matter physics. In superconductors with inversion symmetry, the Cooper pairs must be either in the spin-singlet state or in the spin-triplet state because of the parity conservation law. In contrast, in superconductors without inversion symmetry, mixing of the two states is permitted.¹⁻³ The mixing is determined by spin-orbit coupling (SOC), which is a subject under active scrutiny in various subfields of physics.

Noncentrosymmetric (NCS) superconductors provide a possible new route to spin-triplet superconductivity with a high T_c above 3 K.⁴ Furthermore, they may exhibit novel phenomena such as unusual magnetoelectric effects⁵ or a Fulde-Ferrel-Larkin-Ovchinnikov (FFLO) state with spatially varying pairing functions.⁶ Recently, NCS superconductors have received renewed interests. It has been proposed that they can show topological quantum phenomena such as edge states and non-Abelian statistics,^{7,8} in analogy with topological insulators.^{9,10}

Among various NCS compounds, $\text{Li}_2\text{Pt}_3\text{B}$ ($T_c \sim 2.7$ K)¹¹ is of particular interest. Both $\text{Li}_2\text{Pd}_3\text{B}$ ($T_c \sim 7$ K)¹² and $\text{Li}_2\text{Pt}_3\text{B}$ crystallize in a perovskitelike cubic structure composed of distorted octahedral units of $\text{B}(\text{Pd},\text{Pt})_6$ and are categorized as $P4_332$ (No. 212) in space group.¹³ There is no inversion center in all directions. Many experiments^{4,14-16} have found that $\text{Li}_2\text{Pt}_3\text{B}$ and $\text{Li}_2\text{Pd}_3\text{B}$ show quite striking different properties, except muon spin rotation (μSR).¹⁷ NMR,^{4,14} penetration depth, and specific heat measurements^{15,16} have found that nodes exist in the gap function in $\text{Li}_2\text{Pt}_3\text{B}$ while $\text{Li}_2\text{Pd}_3\text{B}$ is a BCS superconductor. Especially, the NMR results suggested that the spin-triplet state is dominant in $\text{Li}_2\text{Pt}_3\text{B}$.⁴ An early interpretation was that the striking difference in the superconducting properties between isostructural $\text{Li}_2\text{Pt}_3\text{B}$ and $\text{Li}_2\text{Pd}_3\text{B}$ is due to the different strengths of the SOC originating from the different atomic numbers (Z) of Pt and Pd.^{4,15} The atomic SOC is in proportion to Z^2 , which differs by a factor of 3 between Pt and Pd.

Therefore, in the subsequent search for new NCS superconductors, great effort has been made to include heavy elements, which has resulted in the discovery of $\text{Mg}_{10}\text{Ir}_{19}\text{B}_{16}$,¹⁸ Ir_2Ga_9 ,¹⁹ Re_3W ,²⁰ BaPtSi_3 ,²¹ and $\text{Ca}(\text{Ir},\text{Pt})\text{Si}_3$.²² However, a conventional isotropic superconducting gap was found in these compounds,^{19,22,23} and the spin-singlet state was evidenced in $\text{Mg}_{10}\text{Ir}_{19}\text{B}_{16}$.²³ This suggests that Z is not the only parameter determining the singlet-triplet mixing, and other factors await to be revealed.

In this Rapid Communication, we synthesized $\text{Li}_2(\text{Pd}_{1-x}\text{Pt}_x)_3\text{B}$ ($x = 0.2, 0.5, 0.8, 0.84, 0.9$, and 1) and studied the evolution of the superconducting state by ¹¹B, ¹⁹⁵Pt, and ⁷Li NMR measurements. We have also remeasured ¹¹B for the previous $x = 0$ sample¹⁴ at a lower magnetic field, $H = 0.26$ T. In contrast to a naive expectation, we find that the evolution in the pairing symmetry in $\text{Li}_2(\text{Pd}_{1-x}\text{Pt}_x)_3\text{B}$ is not continuous but is abrupt. For $0 \leq x \leq 0.8$, the superconducting state is dominantly a spin-singlet state. However, for $0.9 \leq x$, the spin-triplet state becomes dominant. The $x = 0.84$ compound displays both spin-singlet and spin-triplet characteristics. We find that the local structure changes abruptly for $x > 0.8$ as to increase the extent of inversion-symmetry breaking, which is an effective factor to enhance the strength of SOC as confirmed by our first-principles band calculation. The abrupt increase of the SOC is responsible for the abrupt change in the superconducting properties. The insight obtained here provides a guideline for searching for NCS superconductors with a large spin-triplet component.

Polycrystalline samples of $\text{Li}_2(\text{Pd}_{1-x}\text{Pt}_x)_3\text{B}$ ($x = 0.2, 0.5, 0.8, 0.84, 0.9$, and 1) were prepared in this study by a two-step arc melting method. In the first step, $(\text{Pd}_{1-x}\text{Pt}_x)_3\text{B}$ was synthesized by using Pd(99.95%), Pt(99.999%), and B(99.8%). In the second step, excess Li(99%) by 5%–30% was added to $(\text{Pd}_{1-x}\text{Pt}_x)_3\text{B}$. For $x = 1$, two new samples, #B ($T_c = 2.4$ K) and #C ($T_c = 2.25$ K), whose T_c is close to that reported by Yuan *et al.* ($T_c = 2.43$ K)¹⁵ and Takeya *et al.*

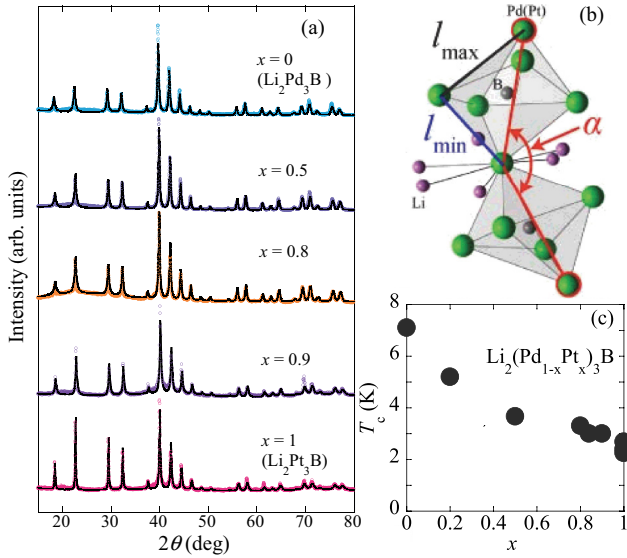


FIG. 1. (Color online) (a) Representative Cu $K\alpha$ XRD charts (circles) with Rietveld analysis (solid curves). The error of the Rietveld fitting (R_F) (Ref. 24) is about 3%. (b) The distorted $\text{B}(\text{Pd,Pt})_6$ octahedral units. α is the angle between the two connected octahedra, and l_{max} (l_{min}) is the longest (shortest) M - M ($M = \text{Pd,Pt}$) bond length. (c) T_c vs Pt content x .

($T_c = 2.17$ K),¹⁶ were made and measured. The previously reported $x = 1$ sample ($T_c = 2.68$ K)⁴ is referred to as $x = 1$ #A. All fresh samples were confirmed to be single phase by powder x-ray diffraction (XRD) [Fig. 1(a)]. Figure 1(b) depicts the $\text{B}(\text{Pd,Pt})_6$ octahedral units whose bond length and angle α is obtained from Rietveld analysis.²⁴ An inductively coupled plasma (ICP) analysis was applied to check the Li:Pd(Pt):B ratio of the resultant samples.²⁵ T_c for each sample at $H = 0$ and a finite H was determined by measuring the inductance of the *in situ* NMR coil. The T_c showed a smooth decrease with increasing x [Fig. 1(c)].

NMR measurements were conducted at $H = 0.26$ T in order to minimize the reduction of T_c by H . The NMR spectra were obtained by a fast Fourier transform of the spin echo taken at the fixed H . The spin-lattice relaxation rate $1/T_1$ was measured for ^{11}B , ^{195}Pt , and ^7Li , and determined by a good fit of the recovery of the nuclear magnetization to a single exponential function. For the alloyed samples, a ^{195}Pt Knight shift was measured, since it is much larger than that of ^{11}B or ^7Li and provides a higher accuracy for broadened spectra due to alloying. Measurements below 1.4 K were carried out with a ^3He - ^4He dilution refrigerator.

The electronic structure calculations were performed by using the full-potential augmented plane-wave plus local orbital method and the Perdew-Burke-Ernzerhof parametrization of the generalized gradient approximation (GGA-PBE) exchange-correlation function²⁶ as implemented in the WIEN2K code.²⁷ The spin-orbital interaction was included by using a second variational procedure. The muffin-tin radii were set to $R_{\text{MT}} = 1.88$ bohrs for B, $R_{\text{MT}} = 2.27$ bohrs for Li, and $R_{\text{MT}} = 2.12$ bohrs for Pd and Pt. The plane-wave cutoff (K_{max}) was determined by $R_{\text{min}}K_{\text{max}} = 7.0$, where R_{min} is the minimal R_{MT} .

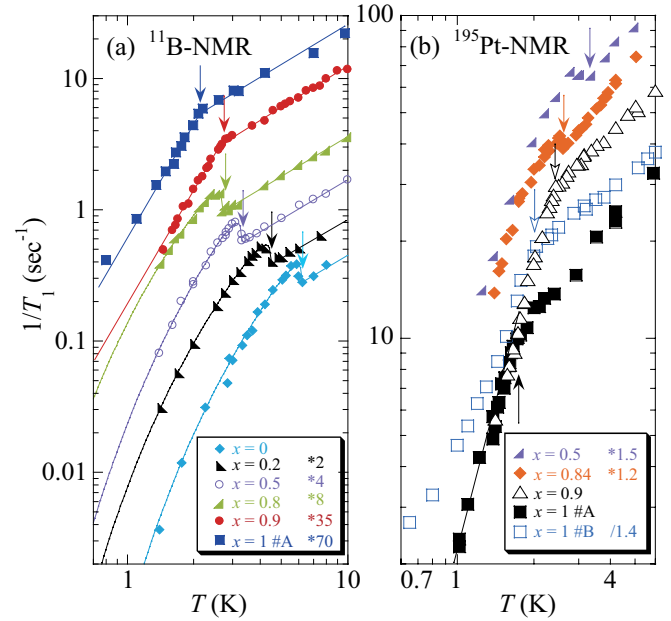


FIG. 2. (Color online) (a) The T dependence of $^{11}(1/T_1)$. The straight lines above T_c indicate the $1/T_1 \propto T$ relation. (b) The T dependence of $^{195}(1/T_1)$ for $x = 0.5, 0.84, 0.9$, and 1 . For both (a) and (b), data were offset vertically for clarity by multiplying or dividing by a number shown in the figure (Ref. 25). Data for $x = 1$ #A ($H = 0.4$ T) were taken from Ref. 4. The arrows indicate T_c under a magnetic field. The straight lines below T_c for $x = 0.9$ and 1 indicate the $1/T_1 \propto T^3$ relation.

Figure 2 shows the temperature (T) dependence of ^{11}B -NMR $1/T_1$ for various x . For $x \leq 0.8$, $^{11}(1/T_1)$ just below T_c is enhanced over its normal-state value, which is a well-known characteristic for an isotropic energy gap. The data below T_c can be fitted by the BCS theory in a procedure described previously,^{14,23} with a resulting gap amplitude $\Delta_0 = 1.70, 1.56, 1.75, 1.50k_B T_c$ for $x = 0, 0.2, 0.5, 0.8$, respectively. The parameter $r = \Delta(0)/\delta$ that characterizes the height of the coherence peak is 1.8, where δ is the energy-level broadening. For $x = 0.9$ and 1 , however, $^{11}(1/T_1)$ shows no coherence peak just below T_c and is in proportion to T^3 , which indicates the existence of line nodes in the gap function.

The contrasting behavior for the two groups of $x \leq 0.8$ and $x \geq 0.9$ is seen in ^{195}Pt NMR as well. In Fig. 2(b) the T dependence of $^{195}(1/T_1)$ for $x = 0.5, 0.84, 0.9$, and 1 is shown. For $x = 0.9$ and 1 , $^{195}(1/T_1)$ shows no coherence peak below T_c and decreases in proportion to T^3 .

To see the spin state of the Cooper pairs, the spin susceptibility χ_s via a Knight shift measurement is the most effective probe. The T dependence of the ^{195}Pt Knight shift (^{195}K) for various x is shown in Fig. 3. The ^{195}K for $x = 0.2, 0.5$, and 0.8 decreases below T_c . It also does so for $x = 0.84$, but the reduction is smaller. For $x = 0.9$ and 1 , however, ^{195}K remains unchanged across T_c .

In order to evaluate quantitatively the evolution of χ_s , one needs to know the Knight shift due to orbital susceptibility K_{orb} since generally $K = K_{\text{orb}} + K_s$, where the spin part K_s is proportional to χ_s or the density of states (DOS) at the Fermi level, $N(E_F)$. ^7Li NMR is useful for estimating $^{195}K_{\text{orb}}$. All ^7Li electrons are in s orbitals and the angular momentum $L = 0$, so that

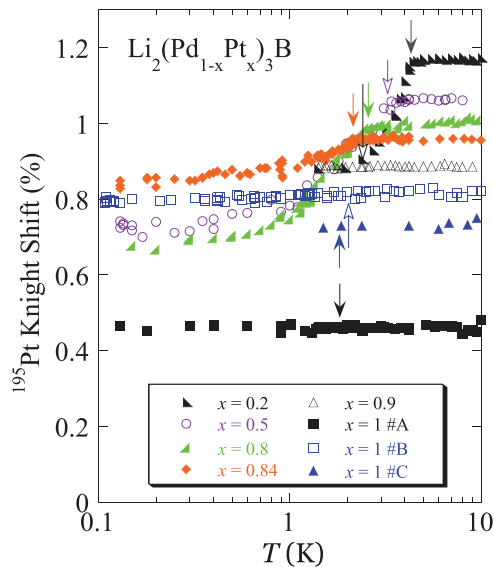


FIG. 3. (Color online) Temperature dependence of the ^{195}Pt Knight shift for various x . The arrows indicate T_c at $H = 0.26$ T except $x = 1$ #A. Data for $x = 1$ #A were taken from Ref. 4 ($H = 0.4$ T) but recalculated using the same magnetic-field calibration as other samples.

$7(1/T_1T) \propto N(E_F)^2$ without an orbital contribution mirrors $^{195}\text{K}_s$. Figure 4 shows the relationship between ^{195}K and $7(1/T_1T)^{1/2}$ for various Pt contents. Indeed, a linear relation between the two quantities is seen. From the extrapolation of the straight line, it is found that $^{195}\text{K}_{\text{orb}} \approx 0.03\%$, then ^{195}K is due predominantly to χ_s .

These results imply that the spin-triplet state is dominant for $x = 0.9$ and 1 and it evolves abruptly above $x = 0.8$. In the intermediate regime, $x = 0.84$, both the spin-singlet and spin-triplet characteristics can be seen. Namely, a small coherence peak is observed and the reduction of $^{195}\text{K}_s$ below T_c is much smaller. Finally, $^{195}\text{K}_s$ not vanishing completely for $x \leq 0.8$

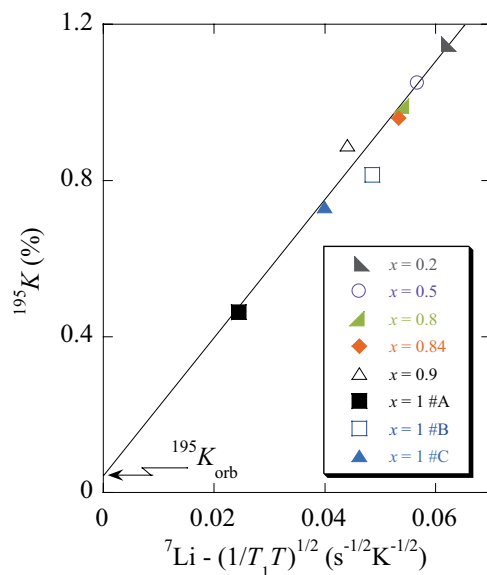


FIG. 4. (Color online) The ^{195}Pt Knight shift in the normal state vs $7(1/T_1T)^{1/2}$ for different Pt contents.

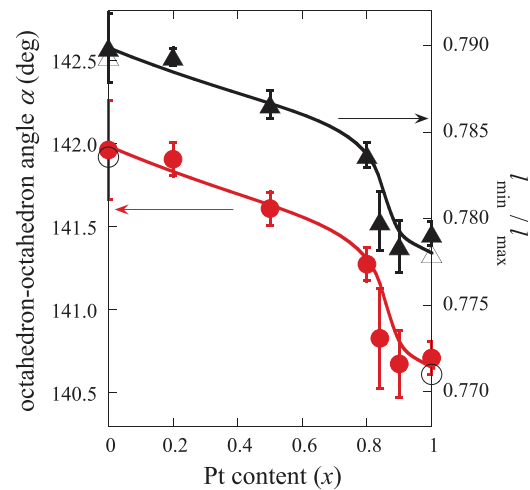


FIG. 5. (Color online) The x dependence of octahedron-octahedron angle α and the bond-length ratio $l_{\text{min}}/l_{\text{max}}$. For $x = 1$, data for sample #B are shown. The open marks are data cited from Ref. 13. The curves are guides to the eyes.

(Ref. 28) may be understood as due to some mixed spin-triplet component and spin-flip scattering by disorder,^{29,30} and even a possible interband susceptibility.³¹

What is the origin of the abrupt increase of the spin-triplet component above $x = 0.8$? Below we show evidence for the SOC increasing abruptly above $x = 0.8$ due to an abrupt increase of the B(Pd,Pt)₆ octahedra distortion. The extent of inversion-symmetry breaking can be measured by two parameters, namely, the angle α between the two connecting octahedra [see Fig. 1(b)] and the ratio $l_{\text{min}}/l_{\text{max}}$, where l_{max} (l_{min}) is the longest (shortest) M - M ($M = \text{Pd}, \text{Pt}$) bond length. In a centrosymmetric structure, $l_{\text{min}}/l_{\text{max}} = 1$ and $\alpha = 180^\circ$. Figure 5 shows the x dependencies of α determined by the general coordinates of Pd(Pt), $12d(\frac{1}{8}, y, \frac{1}{4} - y)$ and Li, and of $l_{\text{min}}/l_{\text{max}}$ determined by y and the lattice constant a .²⁵ Our data for $x = 0$ and 1 are in good agreement with those calculated from

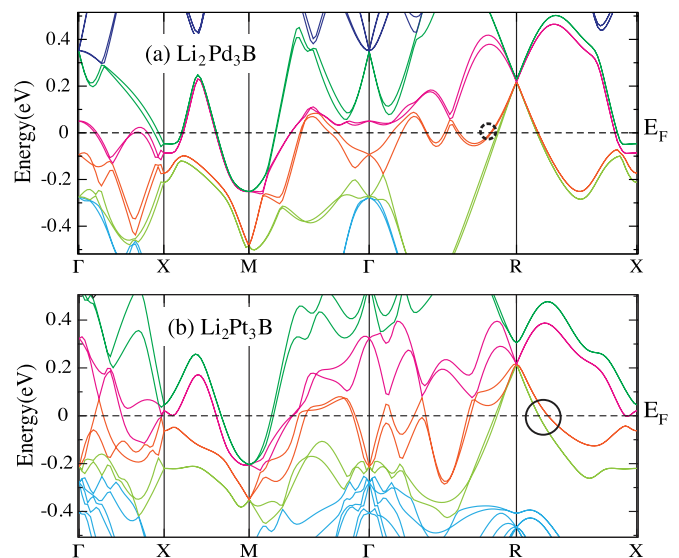


FIG. 6. (Color online) Calculated band dispersion for $\text{Li}_2\text{Pd}_3\text{B}$ and $\text{Li}_2\text{Pt}_3\text{B}$.

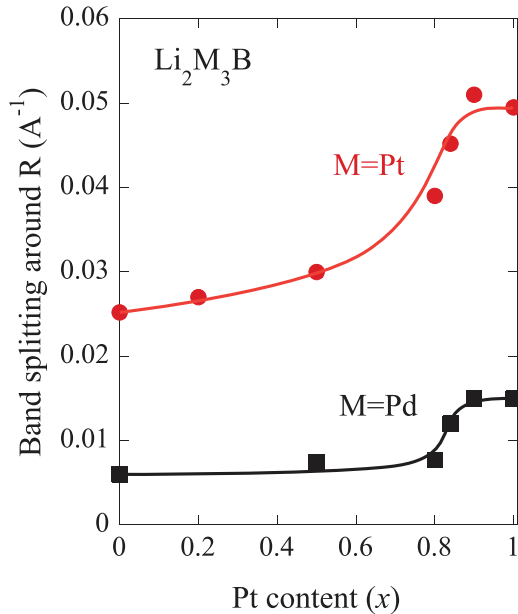


FIG. 7. (Color online) Band splitting around the R point assuming Pt (Pd) occupies all the M sites. The horizontal axis x means that the crystal structure data for $\text{Li}_2(\text{Pd}_{1-x}\text{Pt}_x)_3\text{B}$ are used in the calculation. The curves are guides to the eyes.

y and a reported in Ref. 13. It is found that both α and $\frac{l_{\min}}{l_{\max}}$ show an abrupt reduction above $x = 0.8$.

The band calculation indicates that such an abrupt change in the local crystal structure as to increase the extent of the inversion-symmetry breaking abruptly enhances the SOC. Figure 6 shows the electronic band structure for $\text{Li}_2\text{Pd}_3\text{B}$ and $\text{Li}_2\text{Pt}_3\text{B}$, using the crystal structure data obtained in this work,²⁵ which is in agreement with that reported previously.³² As shown in Fig. 6, the energy bands with SOC are quite complex. Both the splitting due to SOC near E_F around the R and X points are strong. However, only one of SOC-split bands around X point crosses E_F while the two of SOC-split bands around the R point cross E_F . Thus, in order to simply analyze the effect of SOC splitting, below we choose the SOC splitting around R as a typical one.

We iterated the calculation for all compositions x using the lattice parameter and the ionic positions for each x obtained from the Rietvelt analysis but assuming that all M sites are occupied by Pt. The resulting band splitting around the R point along the R - X direction, as marked by the circle in Fig. 6(b), is shown in Fig. 7 by solid circles. Then we performed the same calculation assuming that all M sites are occupied by Pd. In this case, it is the bands around the R point but along

the R - Γ direction, as marked by the dashed circle in Fig. 6(a), that show a pronounced x dependence (squares in Fig. 7). In both cases, the splitting increases abruptly at $x = 0.8$. Also, the eight-degenerate band at the R point around $E = 0.2$ eV is split into a twofold band and a sixfold band, forming a gap between them.²⁵ That gap also shows an abrupt increase at $x = 0.8$.²⁵ This result clearly indicates that, although Pt plays an important role as seen by the difference between the data shown by circles and squares in Fig. 7, the distortion of the $\text{B}(\text{Pt},\text{Pd})_6$ octahedron is more effective in enhancing the SOC, which is called the asymmetric SOC in some literatures. Since the mixing of the spin-singlet and spin-triplet states is determined by the strength of the SOC,^{1,2} the experimental results can be understood as that the asymmetric SOC for $x \geq 0.84$ is so large that the spin-triplet state with line nodes becomes dominant. Although the recently discovered NCS superconductors contain heavy elements such as Pt, Re, or Ir,^{18–23} they lack the structural element found here for $x \geq 0.84$. This appears to be the reason why those NCS materials exhibit conventional superconducting properties. Finally, previous measurements on $\text{Li}_2(\text{Pd}_{0.5}\text{Pt}_{0.5})_3\text{B}$ by μSR (Ref. 17) and the upper critical field³³ highlighting the s -wave gap characteristics are consistent with the present results. On the other hand, some extent of mixing of the spin-triplet component was suggested by analyzing the specific heat¹⁶ and penetration depth³⁴ data on $\text{Li}_2(\text{Pd}_{0.5}\text{Pt}_{0.5})_3\text{B}$. In this regard, theoretical and experimental means to estimate quantitatively the mixed spin-triplet component from the NMR data are desired.

In conclusion, we have studied the evolution of the superconducting state in $\text{Li}_2(\text{Pd}_{1-x}\text{Pt}_x)_3\text{B}$ by NMR. We find that the pairing symmetry changes drastically at $x = 0.8$. For $x \leq 0.8$, the materials are in a predominantly spin-singlet state. However, for $x > 0.8$, unconventional properties due to the mixing of the spin-triplet state appear. The change is caused by an abrupt enhancement of the asymmetric SOC due to an increased distortion of the $\text{B}(\text{Pd},\text{Pt})_6$ octahedral units. Our results indicate that, in addition to a large Z , the structure distortion as to increase the extent of inversion-symmetry breaking is another important, and more effective, factor to increase the mixing of the spin-triplet state.

We thank G. Z. Bao, K. Arima, S. Kawasaki, and Y. Takabayashi for help in experiments and analysis, and K. Miyake, Y. Fuseya, T. Shishido, K. Asayama, and K. Matano for helpful discussions. Work in Okayama was supported by MEXT Grant No. 22103004 and JSPS Grant No. 20244058. Work in Beijing was supported by NSFC (Grants No. 10974231 and No. 11174337) and MOST of China (Grants No. 2011CBA00100 and No. 2011CBA00109).

*ygyao@bit.edu.cn

†zheng@psun.phys.okayama-u.ac.jp

¹L. P. Gorkov and E. I. Rashba, *Phys. Rev. Lett.* **87**, 037004 (2001).

²P. A. Frigeri, D. F. Agterberg, A. Koga, and M. Sigrist, *Phys. Rev. Lett.* **92**, 097001 (2004).

³K. V. Samokhin, *Phys. Rev. Lett.* **94**, 027004 (2005).

⁴M. Nishiyama, Y. Inada, and G.-Q. Zheng, *Phys. Rev. Lett.* **98**, 047002 (2007).

⁵S. Fujimoto, *J. Phys. Soc. Jpn.* **76**, 051008 (2007).

⁶D. F. Agterberg and R. P. Kaur, *Phys. Rev. B* **75**, 064511 (2007); Y. Matsunaga, N. Hiasa, and R. Ikeda, *ibid.* **78**, 220508(R) (2008).

⁷M. Sato and S. Fujimoto, *Phys. Rev. B* **79**, 094504 (2009).

- ⁸Y. Tanaka, Y. Mizuno, T. Yokoyama, K. Yada, and M. Sato, *Phys. Rev. Lett.* **105**, 097002 (2010).
- ⁹X.-L. Qi and S.-C. Zhang, *Rev. Mod. Phys.* **83**, 1057 (2011).
- ¹⁰M. Z. Hasan and C. L. Kane, *Rev. Mod. Phys.* **82**, 3045 (2010).
- ¹¹P. Badica, T. Kondo, and K. Togano, *J. Phys. Soc. Jpn.* **74**, 1014 (2005).
- ¹²K. Togano, P. Badica, Y. Nakamori, S. Orimo, H. Takeya, and K. Hirata, *Phys. Rev. Lett.* **93**, 247004 (2004).
- ¹³U. Eibenstein and W. Jung, *J. Solid State Chem.* **133**, 21 (1997).
- ¹⁴M. Nishiyama, Y. Inada, and G.-Q. Zheng, *Phys. Rev. B* **71**, 220505(R) (2005).
- ¹⁵H. Q. Yuan, D. F. Agterberg, N. Hayashi, P. Badica, D. Vandervelde, K. Togano, M. Sgrist, and M. B. Salamon, *Phys. Rev. Lett.* **97**, 017006 (2006).
- ¹⁶H. Takeya, M. El Massalami, S. Kasahara, and K. Hirata, *Phys. Rev. B* **76**, 104506 (2007).
- ¹⁷H. S. Hafliger, R. Khasanov, R. Lortz, A. Petrovic, K. Togano, C. Baines, B. Graneli, and H. Keller, *J. Supercond. Novel Magn.* **22**, 337 (2009).
- ¹⁸T. Klimczuk, Q. Xu, E. Morosan, J. D. Thompson, and J. D. Thompson, *Phys. Rev. Lett.* **99**, 257004 (2007).
- ¹⁹T. Shibayama *et al.*, *J. Phys. Soc. Jpn.* **76**, 073708 (2007).
- ²⁰J. Yan, L. Shan, Q. Luo, W. Wang, and H. H. Wen, *Chin. Phys. B* **18**, 704 (2009).
- ²¹E. Bauer, R. T. Khan, H. Michor, E. Royanian, A. Grytsiv, N. Melnychenko-Koblyuk, P. Rogl, D. Reith, R. Podloucky, E.-W. Scheidt, W. Wolf, and M. Marsman, *Phys. Rev. B* **80**, 064504 (2009).
- ²²G. Eguchi, D. C. Peets, M. Kriener, Y. Maeno, E. Nishibori, Y. Kumazawa, K. Banno, S. Maki, and H. Sawa, *Phys. Rev. B* **83**, 024512 (2011).
- ²³K. Tahara, Z. Li, H. X. Yang, J. L. Luo, S. Kawasaki, and G.-Q. Zheng, *Phys. Rev. B* **80**, 060503(R) (2009).
- ²⁴F. Izumi and T. Ikeda, *Mater. Sci. Forum* **321–324**, 198 (2000).
- ²⁵See Supplemental Material at <http://link.aps.org/supplemental/10.1103/PhysRevB.86.220502> for ICP analysis results, crystal structure data, the calculated Fermi surface and the enlarged band structure around the R point, and the $1/T_1$ vs T plot without a vertical offset.
- ²⁶J. P. Perdew, K. Burke, and M. Ernzerhof, *Phys. Rev. Lett.* **77**, 3865 (1996).
- ²⁷P. Blaha, K. Schwarz, G. K. H. Madsen, D. Kvasnicka, and J. Luitz, WIEN2K package, available at <http://www.wien2k.at>.
- ²⁸It should be emphasized that the result is not due to a nonsuperconducting component of the sample, since the nuclear magnetization recovery is of a single component and the spectra do not show two-component characteristics.
- ²⁹P. W. Anderson, *Phys. Rev. Lett.* **3**, 325 (1959).
- ³⁰Indeed, the NMR full width at half maximum increases to 12.3 kHz ($x = 0.8$), 12.5 kHz ($x = 0.5$), and 13.1 kHz ($x = 0.2$) from 8.5 kHz for ($x = 0.9$, $x = 1$ #A) and 11 kHz for $x = 0.84$, which suggests that spin-flip scattering can be larger for $0.2 \leq x \leq 0.8$.
- ³¹Such a contribution, $\chi \propto \sum_{k_+, k_-} \frac{f(k_-) - f(k_+)}{E(k_+) - E(k_-)}$, where $+$ and $-$ denote the two split bands, is x insensitive, if any. This is because, qualitatively speaking, the energy splitting $E(k_+) - E(k_-)$ and the population imbalance $f(k_-) - f(k_+)$ are both proportional to the SOC strength.
- ³²K.-W. Lee and W. E. Pickett, *Phys. Rev. B* **72**, 174505 (2005).
- ³³D. C. Peets, G. Eguchi, M. Kriener, S. Harada, Sk. Md. Shamsuzzamen, Y. Inada, G.-Q. Zheng, and Y. Maeno, *Phys. Rev. B* **84**, 054521 (2011).
- ³⁴H. Q. Yuan *et al.*, *Physica B* **403**, 1138 (2008).